2022

A Competent MWCNT-Grafted MnOx/Pt Nanoanode for the Direct Formic Acid Fuel Cells

Islam M. Al-Akraa
The British University in Egypt, islam.ahmed@bue.edu.eg

Ahmad M. Mohammad
Cairo University, ammohammad@cu.edu.eg

Moutaz Mamdouh
The British University in Egypt

Yasser M. Asal

Hindawi
Journal of Chemistry
Volume 2022, Article ID 3762138, 11 pages
https://doi.org/10.1155/2022/3762138

Research Article

A Competent MWCNT-Grafted MnOx/Pt Nanoanode for the Direct Formic Acid Fuel Cells

Islam M. Al-Akraa,[1] **Moutaz M. Mamdouh**,[1] **Yaser M. Asal**,[1] **and Ahmad M. Mohammad**[2]

[1]*Department of Chemical Engineering, Faculty of Engineering, The British University in Egypt, Cairo 11837, Egypt*
[2]*Chemistry Department, Faculty of Science, Cairo University, Cairo 12613, Egypt*

Correspondence should be addressed to Islam M. Al-Akraa; islam.ahmed@bue.edu.eg
and Ahmad M. Mohammad; ammohammad@cu.edu.eg

Received 16 January 2022; Accepted 9 March 2022; Published 25 March 2022

Academic Editor: Samuel Lalthazuala Rokhum

A novel "MnOx/Pt/MWCNT-GC" nanocatalyst is recommended for the electrooxidation of formic acid (EOFA), the principal anodic reaction in the direct formic acid fuel cells (DFAFCs). The sequential (layer-by-layer) protocol was employed to prepare the catalyst through the electrodeposition of Pt (nano-Pt) and manganese oxide (nano-MnOx) nanoparticles onto the surface of a glassy carbon (GC) electrode supported with multiwalled carbon nanotubes (MWCNTs). The nano-MnOx could successfully mediate the mechanism of EOFA by accelerating the charge transfer, "electronic effect". On the other hand, MWCNTs could enhance the catalytic performance by changing the surface geometry that inhibited the adsorption of poisoning CO, which is a typical intermediate in the reaction mechanism of EOFA that is responsible for the potential deterioration of the catalytic performance of DFAFCs. Interestingly with this modification, a significant enhancement in the catalytic activity and stability toward EOFA was achieved. Several techniques will be employed to evaluate the catalyst's morphology, composition, crystal structure, and activity and further to understand the role of each of the nano-MnOx and MWCNTs in the catalytic enhancement.

1. Introduction

The electrooxidation of formic acid (EOFA) has recently gained an incredible attention in the sector of the power generation for potential applications in the direct formic acid fuel cells (DFAFCs) [1, 2]. In fact, with the global movement to address the climate change and sustain affordable and clean electrical power sufficient enough to keep pace with the rapidly growing population and industrialization, it became mandatory to reduce the share of fossil fuels in the power schemes and replace it with alternative greener and renewable technologies [3–5]. The DFAFCs have presented a better scenario for employing small organic liquid fuels as formic acid (FA) instead of H_2 for the power generation for several portable electrical devices. The common risky challenges associating the production, transport, saving, and operation of H_2 have absolutely disappeared with FA while retaining a higher (if compared to 1.2 kWh kg^{-1} and 0.18 kWh L^{-1} of H_2) gravimetric and volumetric energy density of 1.7 kWh kg^{-1} and 2.1 kWh L^{-1} with a little fuel crossover flux via Nafion® membranes [6, 7]. Moreover, DFAFCs offered a competitive theoretical open-circuit potential (1.48 V vs. RHE); excelling that (1.23 V vs. RHE) [8, 9]. Nonetheless, the kinetics (rate and mechanism) of EOFA still encounters the convenient and reliable commercialization of DFAFCs.

Normally, Pt and Pd catalysts are recommended for EOFA, but Pd suffers an inherent instability resulting perhaps from its dissolution in harsh acidic media [10]. On the other hand, Pt experiences severe poisoning with reaction intermediates as CO that is released spontaneously to block most of the Pt active sites. Research is oriented, parallel to minimizing the Pt loading, to overcome its poisoning and to improve its catalytic efficiency toward EOFA. This

was attempted by modifying (doping/alloying) Pt with other metals (Pd, Ni, Co, Cu, Mn, etc.) and/or metal oxides (NiOx, CoOx, CuO, MnOx, etc.) in the presence of a proper substrate to structurally and electronically improve the surface Pt characteristics. In this regard, the modification of Pt with Pd and CeO_2 on multiwall carbon nanotubes (MWCNTs) succeeded to improve the mass activity of the catalyst at least three times while maintaining a seven-fold enhancement in its stability if compared to the commercial PtRu−C catalyst [11]. The role of MWCNTs as a substrate has been investigated separately where a minute amount of MWCNTs could effectively improve the reaction kinetics (1.6 times that of a bare Pt/GC electrode) and mitigate the inherent poisoning of a Pt/GC catalyst toward methanol oxidation [12]. The surface functionalization of AuPd@ZrO_2 nanoparticle-based anodes with MWCNTs inspired as well a remarkable enhancement in the catalyst's activity toward EOFA which depended on the $AuPd_2$ size, Pd surface coverage, PdOx content, and ZrOx stoichiometry [13]. Therein, nonstoichiometric ZrOx nanoparticles were bonded to MWCNTs through C-OOH groups, forming the Zr-O-C bonds while Pd was deposited in a ternary phase (Pd, AuPd, and Au) nanoparticles which formed with ZrOx an intermetallic Pd-O-Zr phase. A remarkable enhancement in the catalyst's durability was attained with the MWCNT-functionalization that enriched the surface with plenty of oxygen containing functional groups which facilitated the desorption of poisoning CO species. An improvement in the electronic properties of the catalyst was also suggested. A similar behavior was reported by Maturost et al. but with CeO_2 and PdPt bimetallic alloy on the surface of MWCNTs [11]. They also suggested a substantial improvement in the kinetics of EOFA and its mass transfer efficiency owing to the catalyst structure (Pd and/or Pt particle size and dispersibility) and its electronic properties that got optimized with the MWCNT-functionalization. Recently, a substrate functionalization with a minute amount of MWCNTs imparted a significant enhancement in the catalytic activity and durability of nano-Pt and NiOx/Pt nanocatalysts for methanol oxidation [12] and EOFA [1], respectively. This extended to tune the mechanism of EOFA exclusively in the desired (low-overpotential) dehydrogenation pathway with a complete suppression for the CO poisoning [1]. Other oxides as manganese oxide (MnOx) are of interest for fuel cell applications as Mn enjoys the existence in multiple stable oxidation states and has a vacant d-orbital that accommodates the electrons involved in the fuel oxidation and, hence, facilitate its reaction kinetics [14–17]. Herein, the excellent catalytic performance of a MnOx/Pt nanostructured anode on a MWCNT-grafted substrate toward EOFA is reported.

2. Experimental

2.1. Catalyst Fabrication. All the chemicals used in this investigation were of analytical grades and were used without prior purifications. A glassy carbon (GC, $d = 3.0$ mm) rod/substrate was used as the working electrode in the catalyst's preparation and in the electrocatalytic measurements. Before using, the GC electrode was polished mechanically with No. 2000 emery paper before repeating polishing with aqueous slurries of successively finer alumina powder (down to 0.06 mm) on a polishing microcloth. Next, the GC electrode was rinsed thoroughly with second distilled water. A spiral Pt wire and an Ag/AgCl/NaCl (3 M) electrode were always used as the counter and reference electrodes, respectively.

To prepare the catalyst, the cleaned GC electrode together with the Pt wire and the Ag/AgCl/NaCl (3 M) reference electrode were all dipped in 0.1 M Na_2SO_4 solution containing 1 mM H_2PtCl_6 and a charge of 10 mC was passed at 0.1 V to deposit nano-Pt onto the GC surface. This electrode will be next abbreviated as the Pt/GC electrode. To deposit MnOx, the Pt/GC electrode served as the working electrode with the regular electrochemical setup and a charge of 16 mC was allowed to pass at 0.1 V from in 0.1 M Na_2SO_4 containing 1.0 mM $Mn(CH_3COO)_2$ solution. This electrode will also be abbreviated as the MnOx/Pt/GC electrode.

To inspect the role of the substrate grafting with MWCNTs, a GC substrate was functionalized with MWCNTs (multiwalled, internal diameter: 5-10 nm, outer diameter: 25 nm, length: 10-30 μm, specific surface area: >55 $m^2 \cdot g^{-1}$, purity: >99.9%) before the deposition of nano-Pt and nano-MnOx. To do this, 10 mg of MWCNTs was mixed with 1 mL 5% Nafion/ethanol solution under sonication for 1 h. Then, 10 μL of the obtained suspension was sprayed on the surface of a GC substrate and left to dry in air at room temperature for another 1 h before washing with double distilled water. The MWCNT-grafted GC electrode was further modified with nano-Pt and nano-MnOx (as mentioned previously), and the catalyst will be termed the MnOx/Pt/MWCNT/GC catalyst.

2.2. Electrochemical Measurements. The electrochemical measurements were carried out in a traditional three-electrode glass cell at room temperature (~25 ± 1°C) using a Bio-Logic SAS potentiostat (model SP-150) operated with EC-Lab software. The catalytic performance of the modified electrodes toward EOFA was investigated in 0.3 M FA solution (pH = 3.5).

2.3. Material Characterization. The morphology and elemental composition were evaluated using a field-emission scanning electron microscope (FE-SEM, Quattro S, Thermo Fisher Scientific USA) whose accelerating voltage extended from 200 V to 30 kV with a magnification range from 6 to 2500000x that equipped with an energy dispersive X-ray spectrometer (EDS, AMETEK USA Element Detector). The crystallographic information was obtained using a high-resolution X-ray diffractometer (XRD-PANalytical X'Pert Pro powder) operated with a Cu anode (wavelength 0.154 nm, maximum 2.2 kW, and 60 kV).

3. Results and Discussions

3.1. Electrochemical Characterization. Electrochemically, the characterizations of the as-prepared catalysts were obtained and useful information about the catalytic ingredients could be obtained. The cyclic voltammograms (CVs) of the Pt/GC,

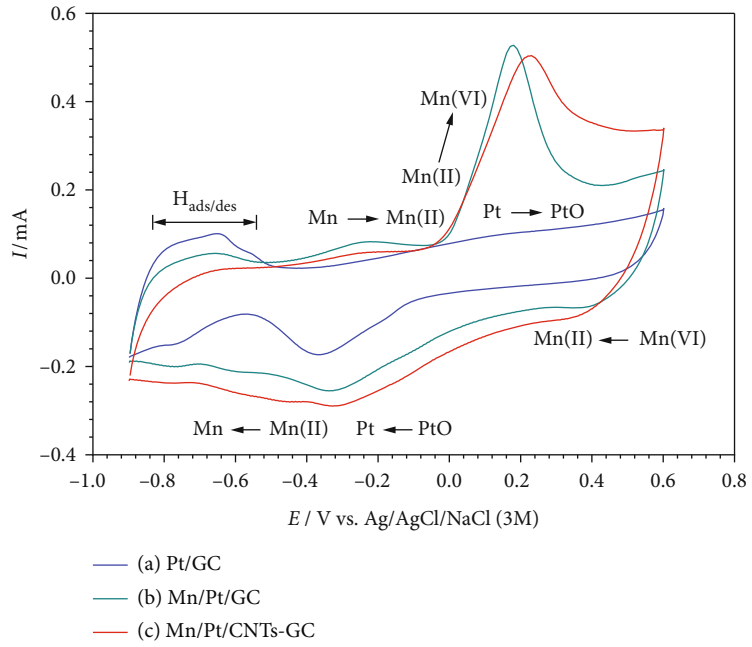

Figure 1: CVs obtained at the (a) Pt/GC, (b) Mn/Pt/GC, and (c) Mn/Pt/CNT-GC electrodes in 0.1 M NaOH. Potential scan rate: 100 mV s^{-1}.

MnOx/Pt/GC, and MnOx/Pt/MWCNT-GC catalysts in 0.5 M NaOH at a potential scan rate of 100 mV s^{-1} are depicted in Figure 1. The typical characteristic behavior of a polycrystalline Pt surface in an alkaline medium was observed at the Pt/GC electrode (Figure 1(a)). The hydrogen adsorption/desorption ($H_{ads/des}$) peaks were observed in the potential range from −0.5 to −0.9 V with the Pt oxidation (Pt→PtO) extending in the anodic potential biasing from −0.2 to 0.6 V. The reduction of PtO (PtO→Pt) was also obvious in the cathodic scan at ca. −0.35 V [14, 18, 19].

At the MnOx/Pt/GC (Figure 1(b)) and MnOx/Pt/MWCNT-GC (Figure 1(c)) catalysts, new features were observed:

(i) Decreases in the charge associating the H_{des} peaks were observed which were consistent with the consumption of the Pt surface in the deposition of nano-MnOx [20]. The decrease in this peak was larger for the MnOx/Pt/MWCNT-GC (Figure 1(c)) catalyst which presumably indicated the role of MWCNTs in the geometrical reorganization of nano-Pt. This reduction in the intensity of the H_{des} peaks did not accompany similar decreases in the intensities of the PtO→Pt peaks as they interfered with the peaks corresponding to the Mn transformations

(ii) Two new anodic peaks were observed at ca. −0.25 and 0.19 V that were assigned, respectively, to the (Mn→Mn (II)) and (Mn (II) to Mn (IV)) oxidations [21]. Their corresponding cathodic peaks appeared, respectively, at ca. 0.4 and−0.27 V

(iii) An observable increase in the double layer capacitance which was attributed to the surface composition change [22]

Table 1: Summary of the electrochemical data extracted from Figure 1.

Electrode	ECSA (cm^2)	θ (%)
Pt/GC	0.65	—
Mn/Pt/GC	0.57	12
Mn/Pt/CNT-GC	0.60	10

To further describe the surface changes after modifying the Pt/GC electrode with nano-MnOx and MWCNTs, two important parameters were extracted from Figure 1. The first parameter is the electrochemical active surface area (ECSA) of the Pt (active component of the catalyst for EOFA) which could be calculated using the following equation [23].

$$\text{ECSA} = \frac{Q_H}{210\,\mu\text{C cm}^{-2}}, \quad (1)$$

where Q_H (μC) is the charge associated with the hydrogen desorption peaks and 210 μC cm^{-2} is the charge required (per specific surface area) for hydrogen desorption from an ideal Pt surface. The decrease in the Pt surface area after the modification with nano-MnOx was thought to originate from, as previously mentioned, the partial deposition of MnOx at the Pt surface.

The second parameter is the Pt surface coverage (θ). This parameter describes how much the Pt was covered after the modification with nano-MnOx and MWCNTs and could be calculated using:

$$\theta\% = \left(1 - \left(\frac{\text{ECSA}_{\text{modified}}}{\text{ECSA}_{\text{unmodified}}}\right)\right) \times 100, \quad (2)$$

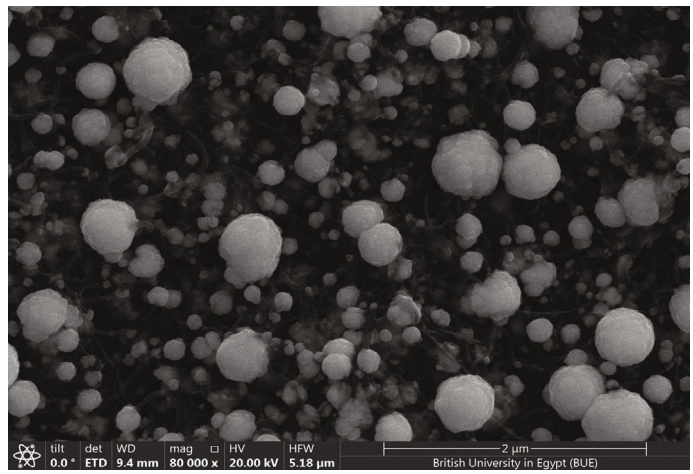

(a)

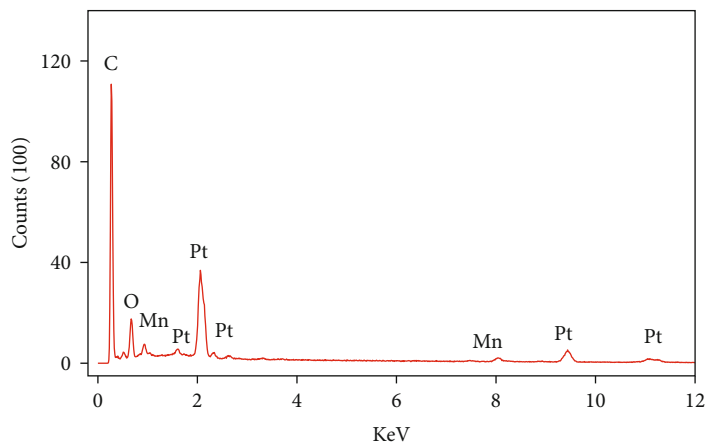

(b)

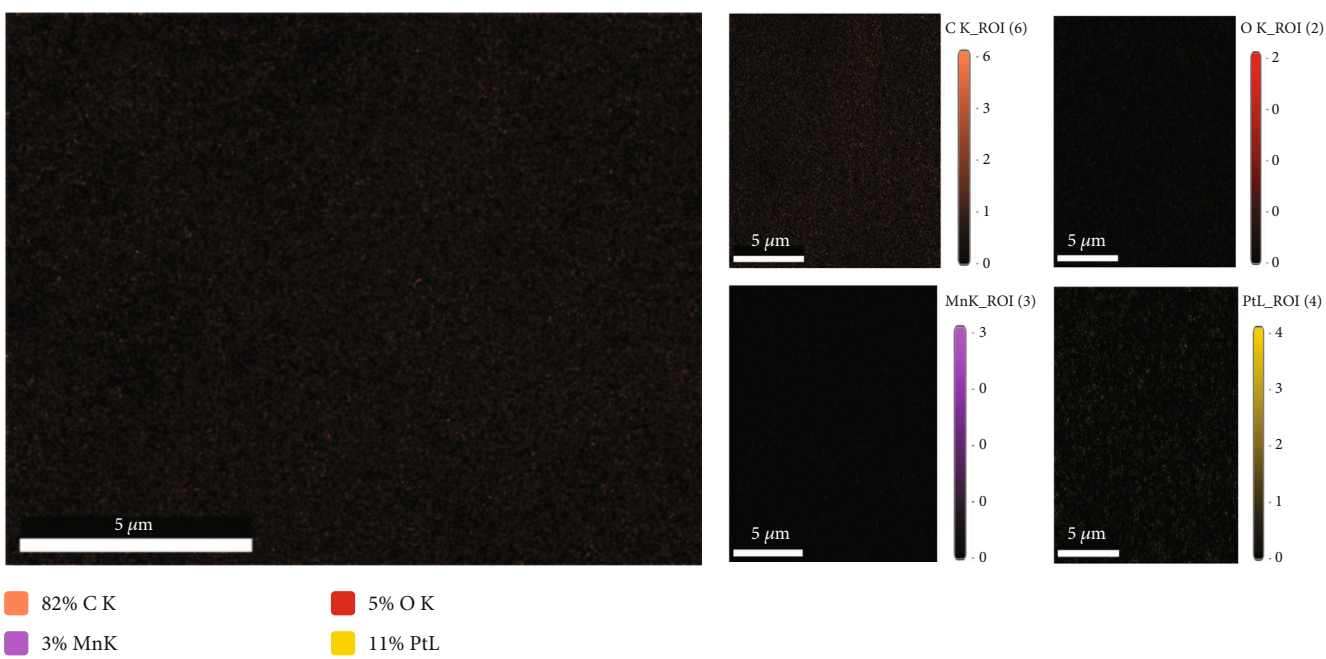

(c)

Figure 2: Continued.

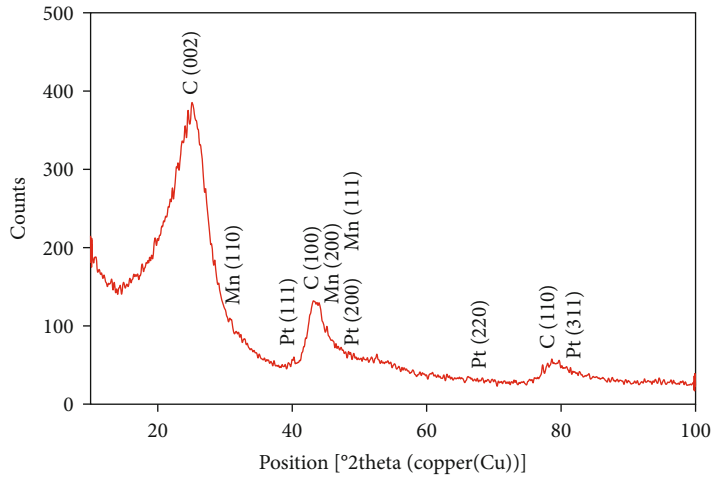

(d)

Figure 2: FE-SEM image (a), EDS analysis (b), elemental mapping (c), and XRD analysis (d) of the Mn/Pt/CNT-GC electrode.

where $ECSA_{modified}$ is the surface area of the modified electrode and the $ECSA_{unmodified}$ is the surface area of the unmodified electrode. Table 1 summarizes the ECSA and surface coverage calculations extracted from Figure 1.

3.2. Material Characterization. Material characterizations of the MnOx/Pt/MWCNT-GC electrode (the best one exhibited the highest catalytic activity and stability toward EOFA, refer to Section 3.3) have been extended to further determine its morphology, composition, and crystal structure. Figure 2 (a) shows the FE-SEM image of the MnOx/Pt/MWCNT-GC electrode. It illustrated the electrodeposition of MnOx and Pt onto the MWCNT-modified GC surface as well-distributed spherical particles having an average size of ca. 85 nm. It is thought that modifying the GC surface with the MWCNTs was responsible for such homogenous loading of Pt and MnOx as previously observed for the deposition of Pt over the MWCNT-GC electrode [12, 22]. In this regard, we would highlight that the other two electrodes (Pt/GC and MnOx/Pt/GC) have been characterized in other previous study and unfortunately they did not exhibit such a homogenous texture like that of the proposed catalyst, MnOx/Pt/MWCNT-GC [14, 15].

Compositionally, the EDS analysis of the MnOx/Pt/MWCNT-GC electrode (Figure 2(b)) confirmed the deposition of the different catalyst ingredients (C, O, Pt, and Mn) and assisted in calculation of their relative ratios (see Table 2). Figure 2(c) additionally provides the elemental mapping for the MnOx/Pt/MWCNT-GC electrode which further confirmed the homogeneous distribution of all catalyst ingredients.

Furthermore, in order to investigate the crystal structure, XRD technique was utilized. Figure 2(d) shows the XRD pattern of the modified MnOx/Pt/MWCNT-GC electrode. Several diffraction peaks were identified at ca. 25°, 43°, and 79° corresponding, respectively, to the (0 0 2), (1 0 0), and (1 1 0) planes of hexagonal C structure [24]. Also the diffraction peaks identified at ca. 40°, 47°, 68°, and 82° belonged, respectively, to the (1 1 1), (2 0 0), (2 2 0), and (3 1 1) planes of the Pt face-centered cubic (fcc) lattice [25]. Moreover, the diffraction peaks appeared at ca. 30°, 45°, and 47° were corresponding, respectively, to the (1 1 0), (2 0 0), and (1 1 1) planes of the cubic β-Mn oxide structure [26].

Table 2: Summary of the electrochemical data extracted from Figure 2(b).

Element	Weight (%)	Atomic (%)	Error (%)
C K	54.36	92.71	7.73
O K	1.99	2.55	32.97
MnK	0.56	0.21	25.43
PtL	43.08	4.52	7.65

3.3. Electrocatalysis of EOFA. Figure 3 shows the CVs of EOFA at the Pt/GC, MnOx/Pt/GC, and MnOx/Pt/MWCNT-GC electrodes in an aqueous solution of 0.3 M formic acid (pH = 3.5). EOFA on Pt-based electrocatalysts proceeds commonly in two different pathways [27–29]. The first pathway involves the dehydrogenation of FA to CO_2 (Equation (3)). This direct route takes place at a low potential domain and so shifts the actual voltage of DFAFCs closer to its theoretical value. That is why the direct pathway was considered the favorable pathway for EOFA [30–32]. Herein, at the Pt/GC electrode (Figure 3(a)), the peak observed at 0.35 V in the anodic scan was assigned to this direct pathway. The corresponding current density of this peak (I_p^d) could be monitored to check the density of the active Pt sites that have participated in this pathway [18, 33].

$$HCOOH_{(aq)} + Pt \longrightarrow Pt + CO_{2(g)} + 2H^+_{(aq)} + 2e^- \quad (3)$$

The second pathway for EOFA is the dehydration of FA (Equation (4)). This will generate CO that will be nonfaradically adsorbed at the Pt surface blocking its active sites. That is why, this indirect pathway was considered the unfavorable pathway for EOFA [34, 35].

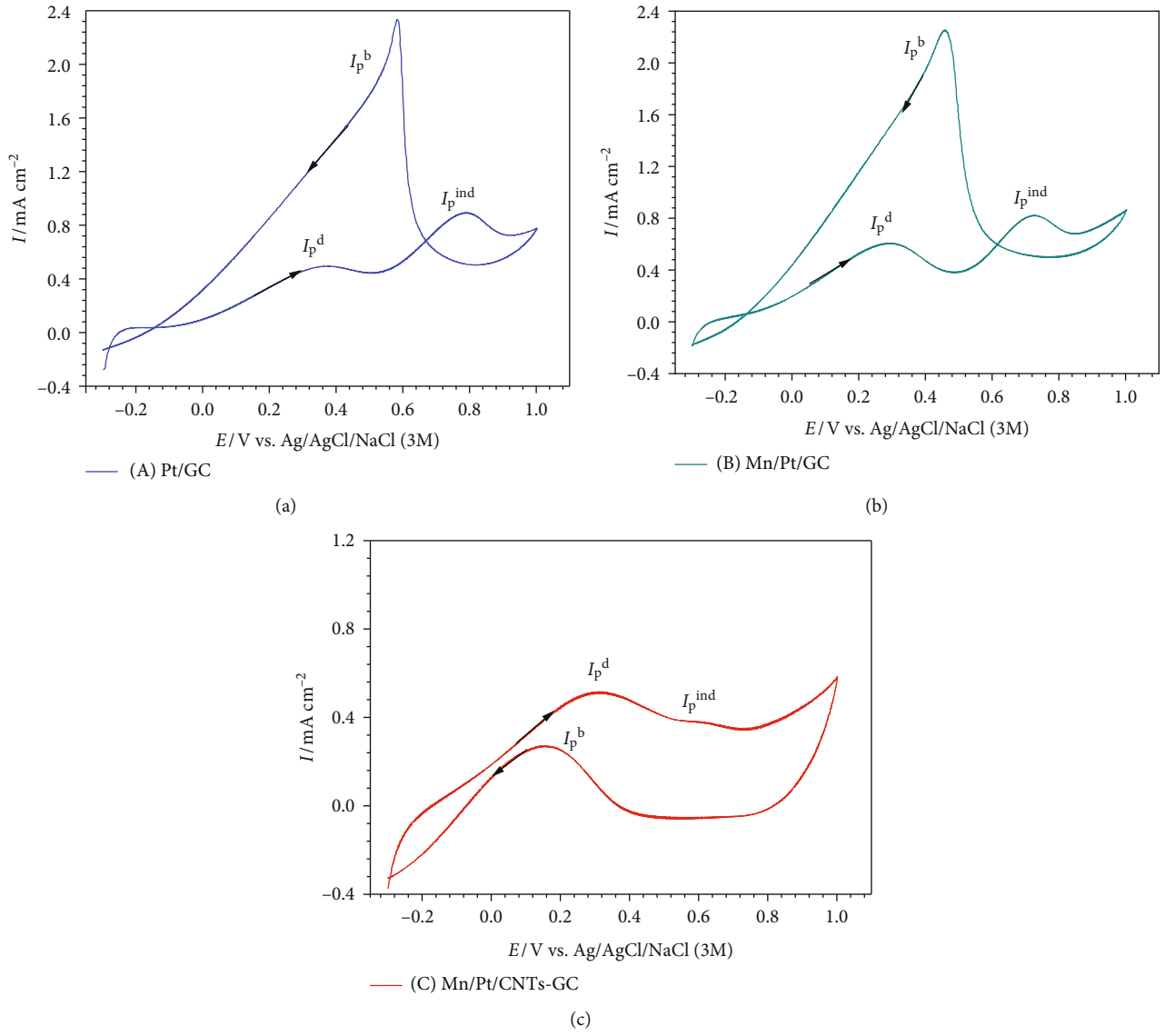

Figure 3: CVs obtained at the (a) Pt/GC, (b) Mn/Pt/GC, and (c) Mn/Pt/CNT-GC electrodes in 0.3 M FA (pH = 3.5). Potential scan rate: 100 mVs^{-1}.

$$HCOOH + Pt \longrightarrow Pt - COads + H_2O \quad (4)$$

With more biasing of the potentials in the anodic direction, the Pt surface will be hydroxylated (Equation (5)) that facilitates the indirect oxidative removal of CO (Equation (6)). The anodic peak observed at ca 0.75 V reflected that pathway, and its corresponding current density (I_p^{ind}) could give a picture about the intensity of CO poisoning of the Pt surface [18, 33].

$$Pt + H_2O \longrightarrow Pt - OH + H^+ + e^- \quad (5)$$

$$Pt - COads + Pt - OH \longrightarrow 2Pt + CO_2 + H^+ + e^- \quad (6)$$

Now after most of the poisoning CO has been oxidized in the forward scan, EOFA could proceed in the backward cathodic scan mainly via the direct pathway (peak at ca. 0.5 V) with a high current density (I_p^b) [36].

After modifying the Pt/GC electrode firstly with nano-MnOx (MnOx/Pt/GC electrode) then with MWCNTs (MnOx/Pt/MWCNT-GC electrode), the degree of catalytic enhancement toward EOFA will be tracked using three parameters, I_p^d/I_p^{ind}, I_p^d/I_p^b, and onset potential of EOFA (E_{onset}). A high I_p^d/I_p^{ind} value indicates the availability of excess active Pt sites free to participate in the direct EOFA at low potential. Meanwhile, a high I_p^d/I_p^b value corresponds to a low level of CO poisoning, whereas a more negative E_{onset} value correlates to a less required overpotential for the reaction, thermodynamics enhancement [37]. At the Pt/GC electrode (Figure 3(a)), the values of I_p^d/I_p^{ind}, I_p^d/I_p^b, and E_{onset} were ca. 0.93, 0.24, and −0.005 V. Although nano-MnOx is not active toward EOFA [20, 38],

Table 3: Summary of the electrochemical data extracted from Figures 3, 5, and 6.

Electrode	I_p^d/I_p^{ind}	I_p^d/I_p^b	E_{onset} (V) @ 0.1 mAcm^{-2}	R_{ct} (kΩ)	Q_{CO} (mC)
Pt/GC	0.93	0.24	−0.005	3.04	1.10
Mn/Pt/GC	3.13	0.50	−0.076	0.75	1.09
Mn/Pt/CNT-GC	18.6	1.20	−0.079	0.92	0.01

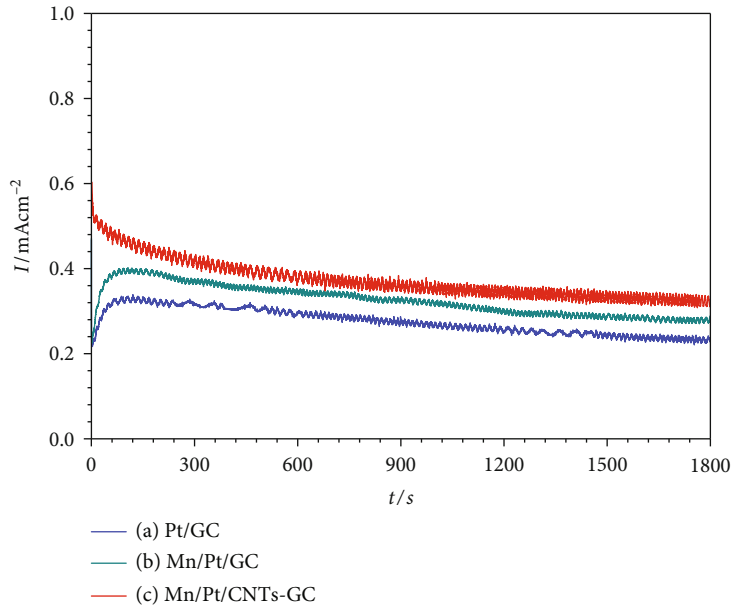

Figure 4: Current transients obtained at the (a) Pt/GC, (b) Mn/Pt/GC, and (c) Mn/Pt/CNT-GC electrodes in 0.3 M FA (pH = 3.5) at 0.25 V.

the catalytic performance of the MnOx/Pt/GC electrode (Figure 3(b)) was higher than that of the Pt/GC electrode toward EOFA in terms of higher I_p^d/I_p^{ind} (3.13) and I_p^d/I_p^b (0.50) and lower E_{onset} (−0.076 V). Fascinatingly after the modification with MWCNTs (which is also inactive toward EOFA [39, 40]) in the case of the MnOx/Pt/MWCNT-GC electrode (Figure 3(c)), the CO poisoning almost disappeared. This was reflected from the highest I_p^d/I_p^{ind} (18.6) and I_p^d/I_p^b (1.2) and the lowest E_{onset} (−0.079 V) values. Table 3 provides a summary of the I_p^d/I_p^{ind}, I_p^d/I_p^b, and E_{onset} values obtained from Figure 3.

Furthermore, the catalytic stability of the modified electrodes was inspected. Figure 4 shows the chronoamperometric (i-t) curves obtained at the Pt/GC (Figure 4(a)), MnOx/Pt/GC (Figure 4(b)), and MnOx/Pt/MWCNT-GC (Figure 4(c)) electrodes in a 0.3 M aqueous solution of FA (pH = 3.5) at a potential of 0.25 V for 1800 s. A poor catalytic stability was observed at the Pt/GC electrode which owned a fast chronic decay in current density, in agreement with previous investigations [31, 32]. Unfortunately, this undesirable decay was kept almost the same for the MnOx/Pt/GC electrode (Figure 4(b)) but surprisingly slowed down to a great extent at the MnOx/Pt/MWCNT-GC electrode (Figure 4(c)). The maximum stability, in terms of the highest and steady-state current density, was obtained at the MnOx/Pt/MWCNT-GC electrode. Till now, modifications with nano-MnOx and MWCNTs were effective in maximizing the catalytic activity and the stability toward EOFA. But the question here is what is the role of each of nano-MnOx and MWCNTs in such observed enhancement? The next section will answer this question.

3.4. Mechanisms of Enhancement. The electrochemical impedance spectroscopy (EIS) was employed to monitor the charge transfer resistance (R_{ct}) of the proposed modified electrodes during EOFA. In principle, R_{ct} that is equivalent to the polarization resistance of the electrochemical system is represented by the diameter of the extrapolated semicircle in the Nyquist diagram [41]. In this regard, the larger the diameter of the semicircle the higher R_{ct}, and consequently, the slower kinetics of the reaction is [42]. Figure 5 shows the Nyquist plots obtained at the Pt/GC, MnOx/Pt/GC, and MnOx/Pt/MWCNT-GC electrodes in a 0.3 M aqueous solution of FA (pH = 3.5) at a potential of 0.2 V in the frequency range (10 mHz to 100 kHz). The fitting has been carried out by the EC-Lab software, and the equivalent circuit of this system was displayed in the inset of Figure 5, where R_{ct}, R_s, and C_{dl} refer to the charge transfer resistance associating EOFA, the solution resistance, and the double layer capacitance, respectively. Figure 5 shows a lower R_{ct} (0.75 and 0.92 kΩ), respectively, at the MnOx/Pt/GC and MnOx/Pt/MWCNT-GC electrodes compared with 3.04 kΩ obtained at the Pt/GC electrode (data are summarized in Table 3).

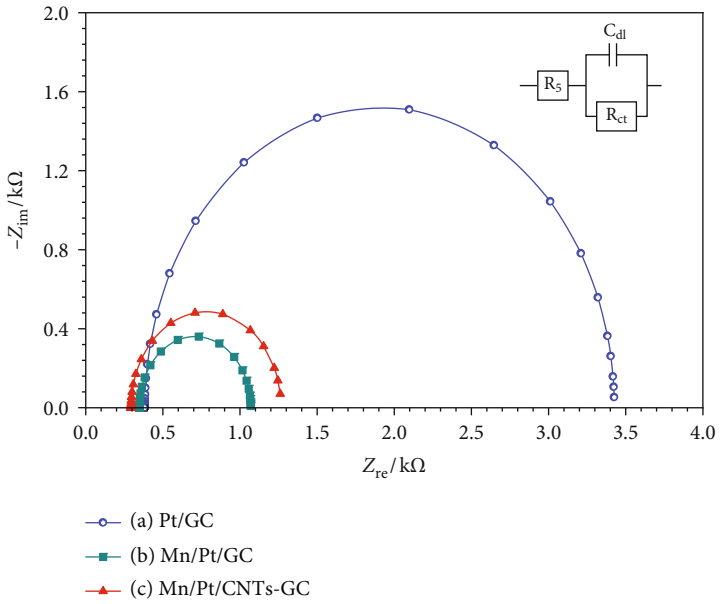

FIGURE 5: Nyquist plots obtained in 0.3 M FA (pH = 3.5) recorded at AC potential amplitude of 0.20 V obtained at the (a) Pt/GC, (b) Mn/Pt/GC, and (c) Mn/Pt/CNT-GC electrodes in 0.3 M FA (pH = 3.5). Frequency range from 10 mHz to 100 kHz.

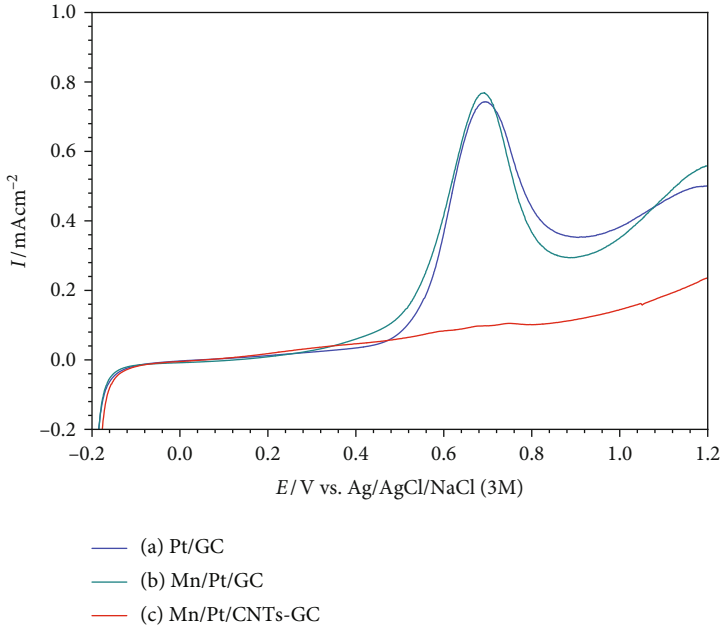

FIGURE 6: LSVs for oxidative CO stripping obtained at the (a) Pt/GC, (b) Mn/Pt/GC, and (c) Mn/Pt/CNT-GC electrodes in 0.5 M Na_2SO_4 (pH = 3.5). Potential scan rate: 50 mVs^{-1}. Before measurements, CO was adsorbed from 0.5 M FA at the open circuit potential for 10 min.

This inferred about a facilitated charge transfer and improved catalytic activity of the MnOx/Pt/GC and MnOx/Pt/MWCNT-GC electrodes toward EOFA. It is important to mention here that the R_{ct} values obtained at the MnOx/Pt/GC and MnOx/Pt/MWCNT-GC electrodes were so close which implies that the modification with MWCNTs did not participate in, rather the nano-MnOx was the catalyst component responsible for, such way of enhancement [20].

To precisely recognize the role of MWCNTs in the catalytic enhancement, CO was chemisorbed from 0.5 M formic acid at open-circuit potential on the Pt/GC, MnOx/Pt/GC, and MnOx/Pt/MWCNT-GC electrodes for 10 min. Then, this adsorbed CO layer was stripped electrochemically in 0.5 M Na_2SO_4 (pH = 3.5) as shown in Figure 6. At the Pt/GC electrode (Figure 6(a)), the surface active sites were blocked at lower potentials because of the adsorbed CO which was next oxidized at ca. 0.70 V. It is worthy to add

here that the charge under the CO oxidation peak (Q_{CO}) reflects the amount of CO adsorbed at lower potentials and so can give a picture about the degree of surface poisoning. Two observations were clear after modifying the Pt/GC electrode with nano-MnOx (MnOx/Pt/GC electrode, Figure 6(b)); the first observation was that the Q_{CO} was almost the same for the Pt/GC and the MnOx/Pt/GC electrodes (1.10 and 1.09 mC, respectively, see Table 3) which suggested that the geometric enhancement, responsible for retarding the CO adsorption at the Pt surface, did not exist [43–45]. The second observation was starting the CO oxidation at the MnOx/Pt/GC electrode at lower potentials (ca. 170 mV negative shift) compared with the Pt/GC electrode. This behavior highlighted the effectiveness of the modification with nano-MnOx and also concluded that such enhancement arose mainly from the modification of the electronic properties of the Pt surface by weakening the Pt-CO bond and thus facilitating the oxidative removal of poisoning CO. [43–45]. This, fortunately, supported the mechanism of enhancement (faster reaction kinetics via a lower R_{ct}) previously proposed from Figure 5. Yet, the role of MWCNTs was not detected, but it will be when looking for the CO stripping curve obtained at the MnOx/Pt/MWCNT-GC electrode (Figure 6(c)). Fascinatingly, at the MnOx/Pt/MWCNT-GC electrode (Figure 6(c)), the Q_{CO} almost disappeared (ca. 0.01 mC). This time, the geometric enhancement was behind such a huge decrease in the amount of adsorbed CO after the modification with MWCNTs. As reported previously, MWCNTs can facilitate the deposition of well-dispersed, nonagglomerated nano-Pt (as in our case, Figure 2(a)) that assisted in retarding the CO adsorption at the Pt surface [12, 22]. This is beside its high electronic conductivity, high corrosion resistance, and good structural, mechanical, and chemical stability [46].

4. Conclusion

The sequential electrodeposition of nano-Pt and nano-MnOx, respectively, at a GC electrode modified with MWCNTs has been carried out aiming to develop a novel anodic catalyst for EOFA. The electrocatalytic activity, stability, and mechanism of enhancement of the best modified electrode (MnOx/Pt/MWCNT-GC) were discussed and compared to the other modified electrodes (Pt/GC and MnOx/Pt/GC). $I_p{}^d/I_p{}^{ind}$, $I_p{}^d/I_p{}^b$, E_{onset}, R_{ct}, and Q_{CO} values supported that the MnOx/Pt/MWCNT-GC electrode exhibited the highest electrocatalytic activity and stability toward EOFA. The mechanisms of enhancement by were thought to come mainly from both electronic (by the modification with nano-MnOx) and geometric (by the modification with MWCNTs) effects.

Data Availability

The data used to support the findings of this study are available from the corresponding author upon request.

Conflicts of Interest

The authors declare that there is no conflict of interest regarding the publication of this paper.

Acknowledgments

This research was supported by the British University in Egypt and Cairo University.

References

[1] I. M. Al-Akraa, A. E. Salama, Y. M. Asal, and A. M. Mohammad, "Boosted performance of NiOx/Pt nanocatalyst for the electro-oxidation of formic acid: A substrate's functionalization with multi-walled carbon nanotubes," *Arabian Journal of Chemistry*, vol. 14, no. 10, article 103383, 2021.

[2] B. A. Al-Qodami, H. H. Alalawy, I. M. Al-Akraa, S. Y. Sayed, N. K. Allam, and A. M. Mohammad, "Surface engineering of nanotubular ferric oxyhydroxide "goethite" on platinum anodes for durable formic acid fuel cells," *International Journal of Hydrogen Energy*, vol. 47, no. 1, pp. 264–275, 2022.

[3] I. M. Al-Akraa, T. Ohsaka, and A. M. Mohammad, "A promising amendment for water splitters: boosted oxygen evolution at a platinum, titanium oxide and manganese oxide hybrid catalyst," *Arabian Journal of Chemistry*, vol. 12, no. 7, pp. 897–907, 2019.

[4] Y. M. Asal, A. M. Mohammad, S. S. A. El Rehim, and I. M. Al-Akraa, "Preparation of co-electrodeposited Pd-Au nanocatalyst for methanol electro-oxidation," *International Journal of Electrochemical Science*, vol. 16, no. 11, article 211133, 2021.

[5] I. M. Al-Akraa, Y. M. Asal, and S. D. Khamis, "Assembling of NiOx/MWCNT-GC anodic nanocatalyst for water electrolysis applications," *International Journal of Electrochemical Science*, vol. 13, pp. 9712–9720, 2018.

[6] L. Yang, G. Li, J. Chang et al., "Sea urchin-like Aucore@Pdshell electrocatalysts with high FAOR performance: coefficient of lattice strain and electrochemical surface area," *Applied Catalysis B: Environmental*, vol. 260, article 118200, p. 118200, 2020.

[7] P. Joghee, J. N. Malik, S. Pylypenko, and R. O'Hayre, "A review on direct methanol fuel cells – in the perspective of energy and sustainability," *MRS Energy & Sustainability*, vol. 2, no. 1, article E3, 2015.

[8] U. B. Demirci, "Direct liquid-feed fuel cells: thermodynamic and environmental concerns," *Journal of Power Sources*, vol. 169, no. 2, pp. 239–246, 2007.

[9] X. Yu and P. G. Pickup, "Recent advances in direct formic acid fuel cells (DFAFC)," *Journal of Power Sources*, vol. 182, no. 1, pp. 124–132, 2008.

[10] I. M. Al-Akraa, Y. M. Asal, S. A. Darwish et al., "Effect of palladium loading on catalytic properties of Pd/GCE for the electro-oxidation of methanol, formic acid, and ethylene glycol," *International Journal of Electrochemical Science*, vol. 17, article 220445, 2022.

[11] S. Maturost, N. Pongpichayakul, P. Waenkaew et al., "Electrocatalytic activity of bimetallic PtPd on cerium oxide-modified carbon nanotube for oxidation of alcohol and formic acid," *Journal of Electroanalytical Chemistry*, vol. 895, article 115445, 2021.

[12] I. M. Al-Akraa, Y. M. Asal, and A. A. Khalifa, "A promising modification of Pt surfaces with CNTs for decreasing

poisoning impact in direct methanol fuel cells," *International Journal of Electrochemical Science*, vol. 14, pp. 8276–8283, 2019.

[13] B. Lesiak, A. Malolepszy, M. Mazurkiewicz-Pawlicka et al., "A high stability AuPd-ZrO $_2$ -multiwall carbon nanotubes supported-catalyst in a formic acid electro-oxidation reaction," *Applied Surface Science*, vol. 451, pp. 289–297, 2018.

[14] Y. M. Asal, I. M. Al-Akraa, A. M. Mohammad, and M. S. El-Deab, "A competent simultaneously co-electrodeposited Pt-MnOx nanocatalyst for enhanced formic acid electro-oxidation," *Journal of the Taiwan Institute of Chemical Engineers*, vol. 96, pp. 169–175, 2019.

[15] G. H. El-Nowihy, A. M. Mohammad, M. M. H. Khalil, M. A. Sadek, and M. S. El-Deab, "Investigating a sequentially assembled MnOx/Pt nanocatalyst as a potential anode for ethylene glycol fuel cells," *International Journal of Electrochemical Science*, vol. 12, pp. 62–73, 2017.

[16] A. M. Mohammad, G. H. El-Nowihy, M. M. H. Khalil, and M. S. El-Deab, "Electrocatalytic oxidation of methanol at nanoparticle-based MnOx/NiOx/Pt ternary catalysts: optimization of loading level and order of deposition," *Journal of the Electrochemical Society*, vol. 161, no. 14, pp. F1340–F1347, 2014.

[17] M. S. El-Deab, G. H. El-Nowihy, and A. M. Mohammad, "Synergistic enhancement of the electro-oxidation of methanol at tailor-designed nanoparticle-based CoOx/MnOx/Pt ternary catalysts," *Electrochimica Acta*, vol. 165, pp. 402–409, 2015.

[18] I. M. Al-Akraa and A. M. Mohammad, "A spin-coated TiOx/Pt nanolayered anodic catalyst for the direct formic acid fuel cells," *Arabian Journal of Chemistry*, vol. 13, no. 3, pp. 4703–4711, 2020.

[19] Y. M. Asal, I. M. Al-Akraa, A. M. Mohammad, and M. S. El-Deab, "Design of efficient bimetallic Pt–Au nanoparticle-based anodes for direct formic acid fuel cells," *International Journal of Hydrogen Energy*, vol. 44, no. 7, pp. 3615–3624, 2019.

[20] A. M. Mohammad, I. M. Al-Akraa, and M. S. El-Deab, "Superior electrocatalysis of formic acid electro-oxidation on a platinum, gold and manganese oxide nanoparticle-based ternary catalyst," *International Journal of Hydrogen Energy*, vol. 43, no. 1, pp. 139–149, 2018.

[21] L. WEN-ZHI, L. YOU-QIN, and H. GUANG-QI, "Preparation of manganese dioxide modified glassy carbon electrode by a novel film plating/cyclic voltammetry method for H_20_2 detection," *Journal of the Chilean Chemical Society*, vol. 54, pp. 366–371, 2009.

[22] I. M. Al-Akraa, Y. M. Asal, and S. A. Darwish, "A simple and effective way to overcome carbon monoxide poisoning of platinum surfaces in direct formic acid fuel cells," *International Journal of Electrochemical Science*, vol. 14, pp. 8267–8275, 2019.

[23] A. L. Ong, K. K. Inglis, D. K. Whelligan, S. Murphy, and J. R. Varcoe, "Effect of cationic molecules on the oxygen reduction reaction on fuel cell grade Pt/C (20 wt%) catalyst in potassium hydroxide (aq, 1 mol dm−3)," *Physical Chemistry Chemical Physics*, vol. 17, no. 18, pp. 12135–12145, 2015.

[24] T. M. Keller, S. B. Qadri, and C. A. Little, "Carbon nanotube formation in situ during carbonization in shaped bulk solid cobalt nanoparticle compositions," *Journal of Materials Chemistry*, vol. 14, no. 20, pp. 3063–3070, 2004.

[25] X. Huang, F. Li, Q. Zhou et al., "In situ synchrotron X-ray diffraction with laser-heated diamond anvil cells study of Pt up to 95 GPa and 3150 K," *RSC Advances*, vol. 5, no. 19, pp. 14603–14609, 2015.

[26] Ş. Özcan, A. Güler, T. Cetinkaya, M. O. Guler, and H. Akbulut, "Freestanding graphene/MnO_2cathodes for Li-ion batteries," *Beilstein Journal of Nanotechnology*, vol. 8, pp. 1932–1938, 2017.

[27] R. Larsen, S. Ha, J. Zakzeski, and R. I. Masel, "Unusually active palladium-based catalysts for the electrooxidation of formic acid," *Journal of Power Sources*, vol. 157, no. 1, pp. 78–84, 2006.

[28] J. D. Lović, A. V. Tripković, S. L. J. Gojković et al., "Kinetic study of formic acid oxidation on carbon-supported platinum electrocatalyst," *Journal of the Electroanalytical Chemistry*, vol. 581, no. 2, pp. 294–302, 2005.

[29] M. Kiani, J. Zhang, Y. Luo et al., "Facile synthesis and enhanced catalytic activity of electrochemically dealloyed platinum–nickel nanoparticles towards formic acid electro-oxidation," *Journal of Energy Chemistry*, vol. 35, pp. 9–16, 2019.

[30] A. Gharib and A. Arab, "Improved formic acid oxidation using electrodeposited Pd–Cd electrocatalysts in sulfuric acid solution," *International Journal of Hydrogen Energy*, vol. 46, no. 5, pp. 3865–3875, 2021.

[31] Z.-Y. Yu, R. Huang, J. Liu et al., "PdPt concave nanocubes directly electrodeposited on carbon paper as high active and durable catalysts for formic acid and ethanol oxidation," *Electrochimica Acta*, vol. 354, article 136654, 2020.

[32] H. Shi, F. Liao, W. Zhu, C. Shao, and M. Shao, "Effective PtAu nanowire network catalysts with ultralow Pt content for formic acid oxidation and methanol oxidation," *International Journal of Hydrogen Energy*, vol. 45, no. 32, pp. 16071–16079, 2020.

[33] M. S. Çögenli and A. B. Yurtcan, "Catalytic activity, stability and impedance behavior of PtRu/C, PtPd/C and PtSn/C bimetallic catalysts toward methanol and formic acid oxidation," *International Journal of Hydrogen Energy*, vol. 43, pp. 10698–10709, 2018.

[34] X. Wen, S. Yin, H. Yin, and Y. Ding, "A displacement dealloying route to dilute nanoporous PtAu alloys for highly active formic acid electro-oxidation," *Electrochimica Acta*, vol. 373, article 137884, 2021.

[35] D. Minudri, A. Y. Tesio, F. Fungo et al., "Surface diffusion of poisoning species during CO and formic acid oxidation on PtAu surface. The key role of the active site," *Journal of Power Sources*, vol. 483, article 229189, 2021.

[36] F.-H. Cho, M.-H. Huang, Y.-M. Chen et al., "Pt-modified dendritic gold as a highly efficient photoelectrocatalyst for the formic acid oxidation reaction," *Applied Surface Science*, vol. 485, pp. 476–483, 2019.

[37] I. M. Al-Akraa, Y. M. Asal, and A. M. Mohammad, "Facile synthesis of a tailored-designed AU/PT nanoanode for enhanced formic acid, methanol, and ethylene glycol electro-oxidation," *Journal of Nanomaterials*, vol. 2019, Article ID 2784708, 2019.

[38] I. M. Al-Akraa, "Efficient electro-oxidation of formic acid at Pd-MnOx binary nanocatalyst: optimization of deposition strategy," *International Journal of Hydrogen Energy*, vol. 42, no. 7, pp. 4660–4666, 2017.

[39] L. Lu, L. Shen, Y. Shi et al., "New insights into enhanced electrocatalytic performance of carbon supported Pd–Cu catalyst

for formic acid oxidation," *Electrochimica Acta*, vol. 85, pp. 187–194, 2012.

[40] I. M. Al-Akraa, A. M. Mohammad, M. S. El-Deab, and B. E. El-Anadouli, "Fabrication of CuOx-Pd Nanocatalyst Supported on a Glassy Carbon Electrode for Enhanced Formic Acid Electro-Oxidation," *Journal of Nanotechnology*, vol. 2018, Article ID 3803969, 2018.

[41] D. V. RIBEIRO, C. A. C. SOUZA, and J. C. C. ABRANTES, "Use of electrochemical impedance spectroscopy (EIS) to monitoring the corrosion of reinforced concrete," *Revista IBRACON de Estruturas e Materiais*, vol. 8, no. 4, pp. 529–546, 2015.

[42] E. Yavuz, K. V. Özdokur, İ. Çakar, S. Koçak, and F. N. Ertaş, "Electrochemical preparation, characterization of molybdenum-oxide/platinum binary catalysts and its application to oxygen reduction reaction in weakly acidic medium," *Electrochimica Acta*, vol. 151, pp. 72–80, 2015.

[43] A. M. Mohammad, G. A. El-Nagar, I. M. Al-Akraa, M. S. El-Deab, and B. E. El-Anadouli, "Towards improving the catalytic activity and stability of platinum-based anodes in direct formic acid fuel cells," *International Journal of Hydrogen Energy*, vol. 40, no. 24, pp. 7808–7816, 2015.

[44] G. A. El-Nagar, A. M. Mohammad, M. S. El-Deab, and B. E. El-Anadouli, "Electrocatalysis by design: enhanced electrooxidation of formic acid at platinum nanoparticles-nickel oxide nanoparticles binary catalysts," *Electrochimica Acta*, vol. 94, pp. 62–71, 2013.

[45] G. Samjeské and M. Osawa, "Current oscillations during formic acid oxidation on a Pt electrode: insight into the mechanism by time-resolved IR spectroscopy," *Angewandte Chemie International Edition*, vol. 44, no. 35, pp. 5694–5698, 2005.

[46] J. Ren, J. Zhang, C. Yang et al., "Pd nanocrystals anchored on 3D hybrid architectures constructed from nitrogen-doped graphene and low-defect carbon nanotube as high-performance multifunctional electrocatalysts for formic acid and methanol oxidation," *Materials Today Energy*, vol. 16, article 100409, 2020.